

Temporal dynamics in the one-dimensional quantum Zakharov equations for plasmas

A. P. Misra,^{1,*} S. Banerjee,^{2,3,†} F. Haas,^{4,‡} P. K. Shukla,^{5,§} and L. P. G. Assis^{6,¶}

¹*Department of Physics, Umeå University, SE-901 87 Umeå, Sweden.*

²*Department of Mathematics, Politecnico di Torino, Turin, Italy.*

³*Micro and Nanotechnology Unit, Techfab s.r.l., Chivasso, Italy.*

⁴*Department of Physics, Umeå University, SE-901 87 Umeå, Sweden.*

⁵*Institut für Theoretische Physik IV, Ruhr-Universität Bochum, D-44780 Bochum, Germany.*

⁶*Grupo de Física Teórica e Matemática Física,
Universidade Federal Rural do Rio de Janeiro BR 465-07,
23851-180, Seropédica, Rio de Janeiro, Brazil.*

(Received 2 Dec., 2009; Revised 15 Feb., 2010; Accepted 16 Feb., 2010)

Abstract

The temporal dynamics of the quantum Zakharov equations (QZEs) in one spatial dimension, which describes the nonlinear interaction of quantum Langmuir waves (QLWs) and quantum ion-acoustic waves (QIAWs) is revisited by considering their solution as a superposition of three interacting wave modes in Fourier space. Previous results in the literature are modified and rectified. Periodic, chaotic as well as hyperchaotic behaviors of the Fourier-mode amplitudes are identified by the analysis of Lyapunov exponent spectra and the power spectrum. The periodic route to chaos is explained through an one-parameter bifurcation analysis. The system is shown to be destabilized via a supercritical Hopf-bifurcation. The adiabatic limits of the fully spatio-temporal and reduced systems are compared from the viewpoint of integrability properties.

PACS numbers: 52.25.Gj; 05.45.Mt; 52.35.Mw.

I. INTRODUCTION

The Zakharov equations (ZEs) are one of the most important models in plasma physics community [1], in which high-frequency Langmuir waves (LWs) are nonlinearly coupled with the low-frequency ion-acoustic waves (IAWs). In this context, the quantum Zakharov equations (QZEs) are the modified version of the classical ZEs, including a quantum correction associated with the Bohm potential [2]. Such QZEs are also deduced from a multiple time-scale technique applied to a set of quantum hydrodynamic (QHD) equations under the quasineutrality assumption. Recent works (see e.g. Refs. [3–6]) indicate that much attention has been paid to investigate the dynamics of such one-dimensional (1D) QZEs. Very recently, a more comprehensive work on the dynamics of LWs has been studied by Haas and Shukla in a three-dimensional quantum Zakharov system [7]. The arrest of Langmuir wave collapse by quantum effects, predicted by a variational approach in Ref. [7], was later confirmed with rigorous estimates and systematic asymptotic expansions by Simpson et al [8].

In contrast to classical ZEs, the QZEs can not be reduced, in the adiabatic limit, to a nonlinear Schrödinger equation (NLSE) [2]. Rather, it follows a coupled system

for the envelope electric field and the density fluctuation, whose complete integrability is not assured. However, the system can be decoupled in the adiabatic as well as semiclassical limit [2, 6], where the solitons can be found to be more stable than in fully degenerate cases [6]. Other recent developments on the QZEs can be found in the literature [3–7, 9–11]. Marklund [3] studied the kinetic theory of LWs interacting with quantum ion-acoustic waves (QIAWs), where it was shown that the combined effects of partial coherence and quantum correction tend to enhance the modulational instability (MI) growth rate [3]. The temporal dynamics of the QZEs has been studied by Haas by means of a variational approach [4]. It has been found that the quantum coupling parameter plays a destabilizing role on localized structures, or Langmuir wave packets. More mathematical treatments on the QZEs are the analysis of the underlying Lie symmetry group [9] and the derivation of some exact solutions [10, 11]. A Galerkin-type approximation was used by Misra et al. [5] to reduce the QZEs to a set of ordinary differential equations (ODEs) for the temporal dynamics. This system was shown to exhibit hyperchaos (more than one positive Lyapunov exponent). However, while qualitatively correct, unfortunately the reduced model considered in this work was flawed by some algebraic inconsistencies.

The primary goal of the present work is to revisit the temporal behavior of the QZEs as a superposition of three interacting wave modes in Fourier space and to rectify the previous results [5]. In addition, the evidence for the existence of periodic limit cycles, chaotic as well as hyperchaotic attractors of the Fourier-mode amplitudes are presented through the analysis of bifurcation diagram, power spectra as well as the Lyapunov exponents. There are relevant differences of the respective

*Electronic address: apmisra@visva-bharati.ac.in; Permanent address: Department of Mathematics, Visva-Bharati University, Santiniketan-731 235, India.

†Electronic address: santo.banerjee@polito.it

‡Electronic address: ferhaas@unisinis.br

§Electronic address: ps@tp4.rub.de.

¶Electronic address: lpgassis@ufrrj.br

periodic, chaotic and hyperchaotic regimes in parameter space. Our findings thus extend both qualitatively and quantitatively the previous results as well as exhibit some new features not reported in the earlier investigations [4, 5].

II. SIMPLIFIED MODEL

The 1D QZEs read [2]

$$i\frac{\partial E}{\partial t} + \frac{\partial^2 E}{\partial x^2} - H^2 \frac{\partial^4 E}{\partial x^4} = n E, \quad (1)$$

$$\frac{\partial^2 n}{\partial t^2} - \frac{\partial^2 n}{\partial x^2} + H^2 \frac{\partial^4 n}{\partial x^4} = \frac{\partial^2 |E|^2}{\partial x^2}, \quad (2)$$

where $E = E(x, t)$ is the envelope electric field and $n = n(x, t)$ is the plasma density fluctuation (measured from its equilibrium value). In Eqs. (1–2), the same set of dimensionless quantities of Ref. [2] is employed. In particular, $H = \hbar \omega_i / \kappa_B T_e$ is a quantum coupling parameter expressing the ratio between the ion plasmon energy and the electron thermal energy, where \hbar is Planck's constant divided by 2π , ω_i is the ion plasma frequency, κ_B is the Boltzmann constant and T_e is the electron fluid temperature. The formal classical limit $H \rightarrow 0$ yields the original Zakharov system [1].

The finite-dimensional temporal dynamics of the QZEs was studied in Ref. [5]. In this investigation, the appearance of hyperchaos was established by means of the derivation of two positive Lyapunov exponents and the analysis of the Kaplan-Yorke dimension. The dynamics of this (low-dimensional) simplified system was considered for a wide parameter range of the system, including the quantum coupling parameter H . However, in the derivation of this simplified model the change of variables in Eqs. (7) and (8) of this work is not fully consistent. Indeed, Eq. (3b) of this paper implies $\dot{a} = -4n_1 \sin \phi$, while Eq. (3c) would imply $\dot{a} = -2n_1 \sin \phi$, using the notations of Ref. [5]. The reason for the contradiction is that the transformations [Eqs. (7), (8) of [5]] do not respect the conservation of plasmon number as given by Eq. (5) of the cited paper. Similar difficulties also appear in the literature about the classical Zakharov system [12, 13], in the derivation of reduced ordinary differential equations simulating the classical ($H = 0$) temporal as well as spatio-temporal system. Hence, in this Section we will rederive the basic set of equations assuming a truncated expansion scheme and produce the correct simplified model. The resulting system is then shown numerically to be compatible with the existence of chaotic as well as hyperchaotic attractors, in qualitative agreement with the conclusions in Ref. [5]. In order to access the low-dimensional dynamical behavior derivable from Eqs. (1–2), we follow Refs. [5] and [13] considering a

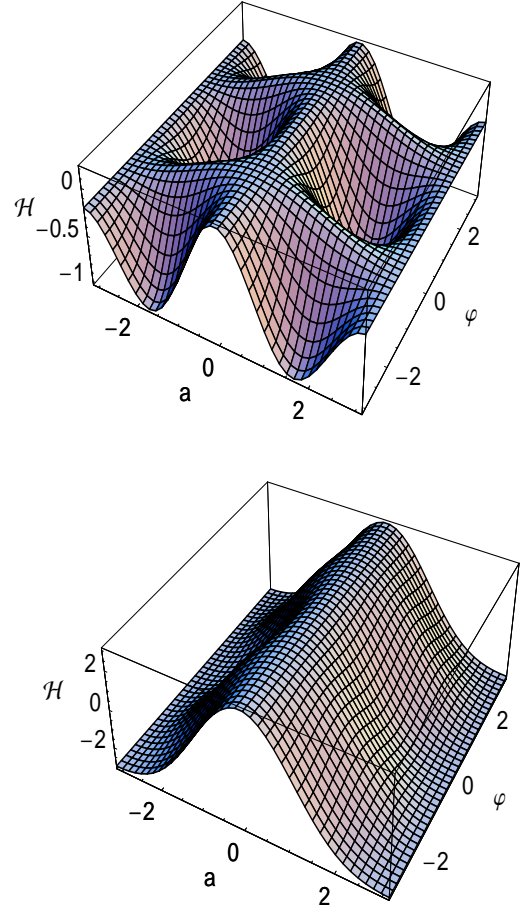


FIG. 1: Hamiltonian function H in Eq. (19), showing distinct qualitative properties for different values of the parameter μ : $\mu = \sqrt{0.5}$ (upper panel), $\mu = \sqrt{3}$ (lower panel).

few-modes expansion through the ansatz

$$E = \sqrt{N} \sin\left(\frac{a}{2}\right) \exp(i\theta_0) + \sqrt{2N} \cos\left(\frac{a}{2}\right) \cos(kx) \exp(i\theta_1), \quad (3)$$

$$n = N + n_1 \cos(kx), \quad (4)$$

where N is the conserved plasmon number, k is the fixed wave-number of the excitation and $a = a(t)$, $\theta_0 = \theta_0(t)$, $\theta_1 = \theta_1(t)$ and $n_1 = n_1(t)$ are real time-dependent quantities. It is important to notice that Eq. (3) implies $|E|^2 = N + \text{oscillatory terms}$, in agreement with the conservation of plasmon number.

Inserting Eqs. (3–4) into Eqs. (1–2) and computing the zero wave-number term and the coefficient of the term proportional to $\cos(kx)$ yields four equations, corresponding to the real and imaginary parts. Further, the higher-order harmonics proportional to $\cos(2kx)$ are disregarded, in the spirit of the present few modes approximation. The real and the imaginary parts of the

independent term gives

$$\dot{a} = -\sqrt{2} n_1 \sin \varphi, \quad (5)$$

$$\dot{\theta}_0 = -N - \frac{\sqrt{2}}{2} n_1 \cos \varphi \cot \left(\frac{a}{2} \right), \quad (6)$$

where the ‘dot’ represents derivative with respect to time t and

$$\varphi = \theta_0 - \theta_1. \quad (7)$$

Now, considering the real part of the coefficient of the term proportional to $\cos(kx)$ we get

$$\dot{\theta}_1 = -N - k^2(1 + H^2 k^2) - \frac{\sqrt{2}}{2} n_1 \cos \varphi \tan \left(\frac{a}{2} \right). \quad (8)$$

The imaginary part of the coefficient or the term proportional to $\cos(kx)$ provides no further information. The combination of Eqs. (6-8) gives

$$\dot{\varphi} = k^2(1 + H^2 k^2) - \sqrt{2} n_1 \cos \varphi \cot a. \quad (9)$$

To close the system, it is necessary to substitute the ansatz of Eqs. (3-4) also into Eq. (2). Ignoring again higher-order harmonics yields

$$\ddot{n}_1 + k^2(1 + H^2 k^2) n_1 = -\sqrt{2} N k^2 \cos \varphi \sin a. \quad (10)$$

The system of Eqs. (5),(9) and (10) provides a finite-dimensional closed set of ordinary differential equations for a , φ and n_1 , whose properties will be analyzed numerically in the next Section.

Of particular interest is the case where the density fluctuations respond adiabatically to excitations. In this situation the second derivative term in Eq. (10) can be neglected, yielding

$$n_1 = -\frac{\sqrt{2} N}{1 + H^2 k^2} \cos \varphi \sin a. \quad (11)$$

Inserting this last result into Eqs. (5) and (9), we get the two-dimensional dynamical system

$$\dot{a} = \frac{N}{1 + H^2 k^2} \sin 2\varphi \sin a, \quad (12)$$

$$\dot{\varphi} = k^2(1 + H^2 k^2) + \frac{2N}{1 + H^2 k^2} \cos^2 \varphi \cos a. \quad (13)$$

Actually, Eqs. (12) and (13) contain only one relevant free parameter μ , as can be proved by introducing the rescaled time variable

$$\tau = \frac{N t}{1 + H^2 k^2}, \quad (14)$$

so that

$$da/d\tau = \sin 2\varphi \sin a, \quad (15)$$

$$d\varphi/d\tau = \mu^2 + 2 \cos^2 \varphi \cos a, \quad (16)$$

where

$$\mu = \frac{k(1 + H^2 k^2)}{\sqrt{N}}. \quad (17)$$

In this formulation, the role of quantum effects, contained in the free parameter H , are hidden in the rescaled time τ and also in μ . Thus, the quantum effects tend to slow down the dynamics, since a larger H causes $d\tau/dt$ to become smaller in magnitude. Moreover, it follows from Eq. (16) that the fixed points can exist only when $\mu \leq \sqrt{2}$. But, since μ is a monotonically increasing function of H , the conclusion is that quantum effects tend to suppress the existence of equilibrium points.

In addition, Eqs. (15-16) form a completely integrable dynamical system, as can be better seen in writing it in the generalized Hamiltonian form

$$\frac{da}{d\tau} = J \frac{\partial \mathcal{H}}{\partial \varphi}, \quad \frac{d\varphi}{d\tau} = -J \frac{\partial \mathcal{H}}{\partial a}, \quad (18)$$

where $J = \csc a$ and the first integral H playing the role of Hamiltonian function is

$$\mathcal{H} = \mu^2 \cos a - \cos^2 \varphi \sin^2 a. \quad (19)$$

The system (18) can be written in canonical Hamiltonian form using Darboux coordinates $(u, v) = (-\cos a, \varphi)$, so that $du/d\tau = \partial \mathcal{H}/\partial v$, $dv/d\tau = -\partial \mathcal{H}/\partial u$. Most importantly, Eq. (18) is manifestly non-chaotic. Notice, however, that the level surfaces of the constant of motion H are not compact, and thereby violating a necessary condition for Liouville integrability. In addition, the Poisson structure is singular in the sense that J is not well-defined for $a = l\pi$, where l is an integer. Figure 1 exhibits some typical graphs of H for $\mu = \sqrt{0.5}$ and $\mu = \sqrt{3}$ showing distinct qualitative properties of the constant of motion.

On the other hand, the adiabatic limits of the simplified finite-dimensional system and the original infinite-dimensional system are to be compared. For the infinite-dimensional system, the adiabatic limit is get disregarding the second-order time derivative of the density fluctuation in Eq. (2). The resulting equations are

$$i \frac{\partial E}{\partial t} + \frac{\partial^2 E}{\partial x^2} + |E|^2 E = H^2 \left(\frac{\partial^4 E}{\partial x^4} + E \frac{\partial^2 n}{\partial x^2} \right), \quad (20)$$

$$H^2 \frac{\partial^2 n}{\partial x^2} - n = |E|^2, \quad (21)$$

which in the formal classical limit ($H \rightarrow 0$) reduce to the usual NLSE, which is well-known to be completely integrable. However, in the quantum case, the adiabatic limit still shows a coupled nonlinear system, whose properties are not yet completely known. In contrast, the simplified dynamics associated to the present few-modes ansatz has shown to be integrable. Notice that the system (20-21) can be decoupled taking both the semiclassical ($H \ll 1$) as well as adiabatic limits, so that the substitution $n = -|E|^2$ is allowed in the right-hand side

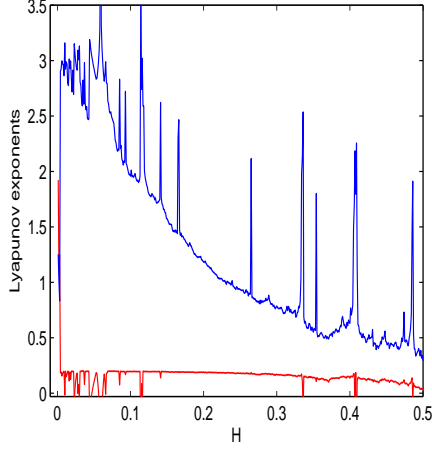


FIG. 2: Two largest Lyapunov exponents with respect to H and for constant $N = 1.5$ and $k = 0.8$.

of Eq. (20). In this case one obtains

$$i \frac{\partial E}{\partial t} + \frac{\partial^2 E}{\partial x^2} + |E|^2 E = H^2 \left(\frac{\partial^4 E}{\partial x^4} - E \frac{\partial^2 |E|^2}{\partial x^2} \right). \quad (22)$$

Equation (22) can be used as the starting point for studying quantum perturbations of the classical NLS soliton solutions [6].

III. NUMERICAL RESULTS

The system of Eqs. (5), (9) and (10) can be recast as

$$\dot{x}_1 = -\sqrt{2} x_3 \sin x_2, \quad (23)$$

$$\dot{x}_2 = k^2 (1 + H^2 k^2) - \sqrt{2} x_3 \cos x_2 \cot x_1, \quad (24)$$

$$\dot{x}_3 = x_4, \quad (25)$$

$$\dot{x}_4 = -k^2 (1 + H^2 k^2) x_3 - \sqrt{2} N k^2 \cos x_2 \sin x_1, \quad (26)$$

where, for convenience, we have redefined the variables as $a = x_1, \varphi = x_2, n_1 = x_3, \dot{n}_1 = x_4$.

Eqs.(23–26) were numerically solved by using the sixth order Runge-Kutta-Fehlberg scheme with the step length $h = 0.01$ and initial values as $x_1 = 0.1, x_2 = 0.2, x_3 = 0.3, x_4 = 0.1$. A Monte-Carlo search on the parameter space was conducted to find the possible dynamics of the system, namely periodic, chaotic or hyperchaotic regimes. In order to establish the existence of irregular dynamics we have investigated the Lyapunov exponents spectra [14]. Chaos or hyperchaos is characterized by the presence of one or two positive largest Lyapunov exponents respectively. It is sufficient to calculate only the three largest Lyapunov exponents. These largest Lyapunov exponents were calculated by integrating Eqs. (23–26) in order to have average estimates of them over the attractors [15]. Figure 2 shows examples of two largest

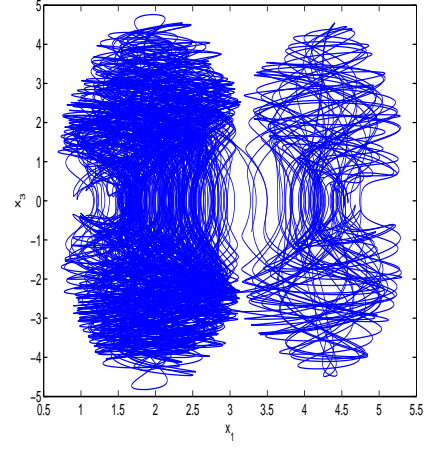


FIG. 3: Hyperchaotic phase portrait of the system (23)-(26) in the $x_1 - x_3$ plane for $H = 0.2, N = 1.5$ and $k = 0.8$.

Lyapunov exponents with respect to the quantum parameter H and for constant $N = 1.5$ and $k = 0.8$ such that $\mu \leq \sqrt{2}$ is satisfied. We observe that the system is chaotic (one positive exponent) for a small range of H , while it is hyperchaotic (two positive exponents) for a wide range of values of H . In the classical case, i.e., for $H = 0$, we also find two positive Lyapunov exponents indicating the hyperchaotic features even in the classical ZEs [1] as well. It is to be noted that the system may experience some other features at the points where some peaks of the first (maximum) Lyapunov exponent seem to be correlated with the depletions of the second exponent. However, since the variations of the exponents are shown with respect to a system parameter, namely H , there may be a possibility for the existence of chaos rather than the hyperchaotic orbits at those points, especially where the second Lyapunov has negative peaks. Figure 3 shows an example of the hyperchaotic dynamics of the system in the $x_1 - x_3$ plane for $H = 0.2, N = 1.5$ and $k = 0.8$. It seems to show an intermittent switching between two regions of the phase space, one to the left and other to the right of $x_1 \approx 3.2$. These can be verified from the corresponding time series for x_1 and x_3 as shown in Fig. 4. Here the upper panel clearly explains this intermittency near $x_1 = 3.2$, and both the time series show the aperiodic nature of the system which are very common in the context of chaotic dynamics. The chaotic dynamics of the system can be established by calculating the power spectrum corresponding to the variable x_3 . Here one can measure the power spectrum as the square of the modulus of the complex Fourier coefficients corresponding to x_3 with frequency as the inverse of the period of the signal [16]. However, measuring the amplitude of the pulse gives rise a slight modification of the power of the same obtained by using the Fast Fourier Transform (FFT). The latter is used to compute the discrete Fourier Transform (DFT) of the signal, as well as the magnitude

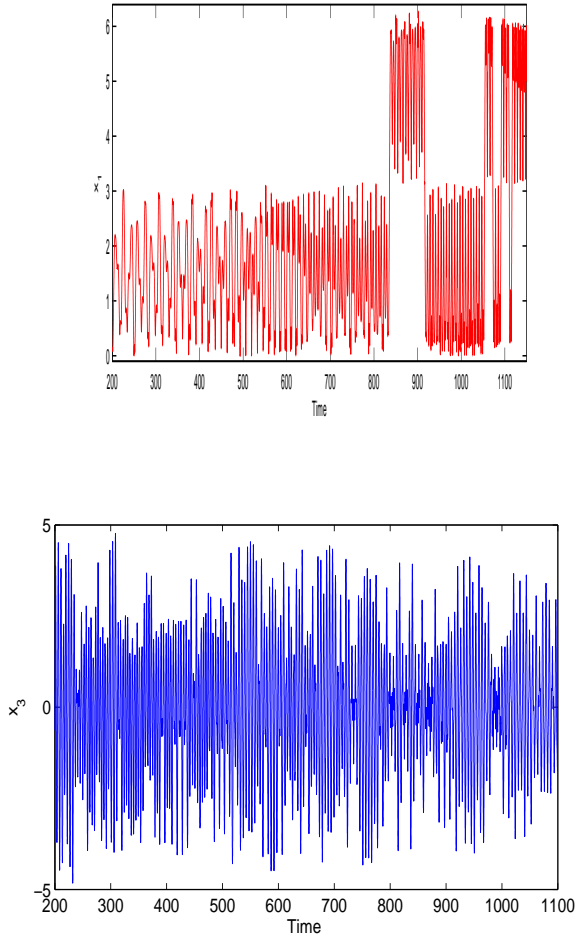


FIG. 4: The time series corresponding to the variables x_1 (upper panel) and x_3 (lower panel). The parameter values are the same as in Fig. 3.

and phase of the transformed signal [17]. The ‘abs’ function is used to obtain the magnitude of the data and the ‘angle’ function to obtain the phase information [18], and unwrap in order to remove the phase jumps greater than π to their 2π complement. These are illustrated in Fig. 5. This figure clearly shows the chaotic dynamics of the waveforms with low-frequency and high amplitudes, as well as exhibits the broadband spectral features of the system. The route to chaos from a single periodic orbit can be explained by means of a one-parameter bifurcation analysis in the domains of dynamical variables. We have considered one fixed value of $H = 0.2$, two different values of k , namely $k = 0.9, 0.95$ and allowed the plasmon number N to vary so as to satisfy the inequality $\mu \leq \sqrt{2}$.

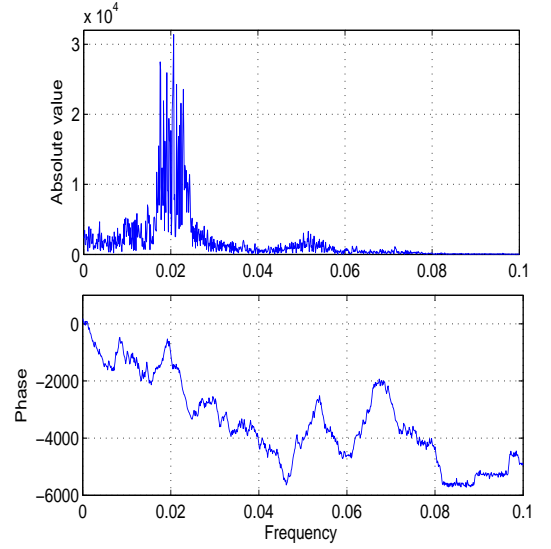


FIG. 5: The amplitude (absolute value, see the upper panel) and the phase (lower panel) of the hyperchaotic signal corresponding to the variable x_3 . The parameter values are the same as in Fig. 3.

The three-dimensional pictorial views of the bifurcation diagram with x_1 , x_3 and N are shown in Fig. 6 for distinct values of k . These explain that the system loses its stability through a supercritical Hopf-bifurcation (hb), which gives the birth to periodic limit cycles at $N \approx 0.78$ for $H = 0.2, k = 0.9$ (upper panel) and $N \approx 0.6$ for $H = 0.2, k = 0.95$ (lower panel). The nature of the supercritical Hopf-bifurcation can be seen in the x_1 - x_2 plane from Fig. 7 for $N = 1.5$, $H = 0.2$ and different k : (i) $k = 0.3$ (upper panel) and (ii) $k = 0.5$ (lower panel). Notice that in the case of Hopf-bifurcation, we have generated a program with varying k from $k = 0.1$ to 1.0 . Figure 7 shows illustrations of two different values of k . The trajectories in both the upper and lower panel of Fig. 7 are generated with different initial conditions, and finally they converge to attracting or repelling limit cycles. In both the cases the initial values are taken from the unstable sets. For values of k larger than $k = 0.5$ no more attracting or repelling limit cycle is found to coexist. From Fig. 7 one can also observe that a limit cycle (the blue curves or e.g., the orbits appeared first from the bottom at $x_1 < 0$ and at $x_1 > 0$) is surrounded by the unstable equilibriums (red colored curves). To further examine the chaotic features, one can also calculate the Fourier transform of the signal [16] corresponding to the variable x_1 . Figure 8 represents the distribution of the Fourier coefficients in the complex plane corresponding to the chaotic signal x_1 for $H = 0.2, N = 1.5$ and $k = 0.8$. It shows how wide and dense are the Fourier coefficients in the complex plane. This distribution could be useful to quantify chaos from numerical points of view. However, the detail analysis is beyond the scope of the present

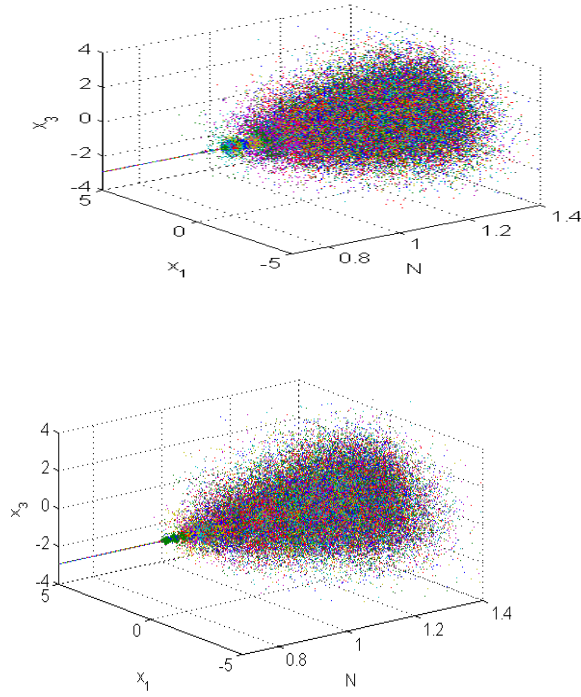


FIG. 6: The snap shots of an animated movie showing the three-dimensional views of the bifurcation diagrams with variation of the parameter N and for a fixed $H = 0.2$. Two different values of k are: $k = 0.9$ (upper panel) and $k = 0.95$ (lower panel). Different colors may correspond to the pixels of different projections on the “floor”.

work.

IV. CONCLUSION

The nonlinear interaction of quantum Langmuir waves and quantum ion-acoustic waves is analyzed in terms of a superposition of three interacting wave modes in Fourier space. Previous works on both classical [12, 13] and quantum [5] Zakharov equations have been rectified and modified. The chaotic behaviors of the reduced temporal system have been identified by the analysis of Lyapunov exponent spectra as well as by the analysis of power spectrum. The hyperchaos has been characterized by the presence of two positive Lyapunov exponents. Also, the route to chaos from a single

periodic orbit is analyzed by means of one-parameter bifurcation analysis. Moreover, the reduced temporal dynamics is shown to be integrable in the adiabatic limit. This is in contrast to the adiabatic limit of the spatiotemporal dynamics described by the QZEs whose integrable properties deserves further study; whereas the finite-dimensional reduced system is shown to evolve into periodic, chaotic as well as hyperchaotic orbits [5].

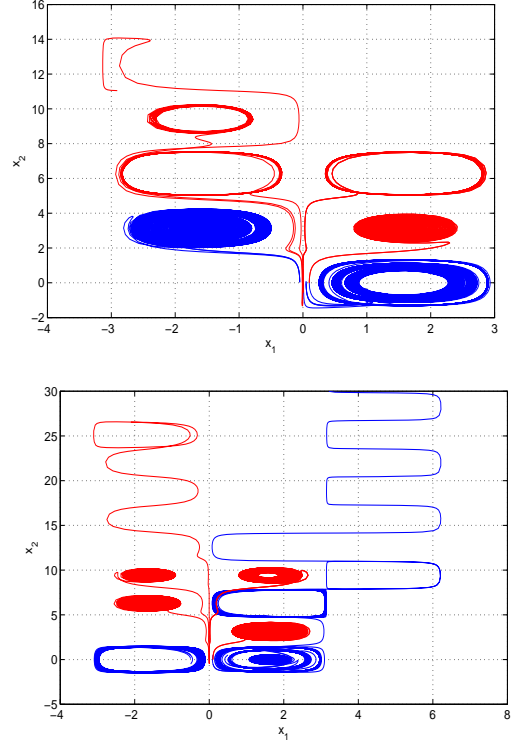


FIG. 7: Supercritical Hopf-bifurcation in the $x_1 - x_2$ plane for $N = 1.5$, $H = 0.2$ and different k : (i) $k = 0.3$ (upper panel) (ii) $k = 0.5$ (lower panel).

To conclude, we believe that the results presented in this work would be helpful for better understanding the salient features of such 1D QZEs.

ACKNOWLEDGMENTS

A. P. M. is grateful to the Kempe Foundation, Sweden for support. F.H. acknowledges support from Umeå University and the Kempe Foundation.

-
- [1] V. E. Zakharov, Sov. Phys. J. Exp. Theor. Phys. 35, 908 (1972).
 - [2] L. G. Garcia, F. Haas, L. P. L. de Oliveira, and J. Goedert, Phys. Plasmas 12, 012302 (2005).

- [3] M. Marklund, Phys. Plasmas 12, 082110 (2005).
- [4] F. Haas, Phys. Plasmas 12, 042309 (2007).
- [5] A. P. Misra, D. Ghosh, and A. R. Chowdhury, Phys. Lett. A 372, 1469 (2008).

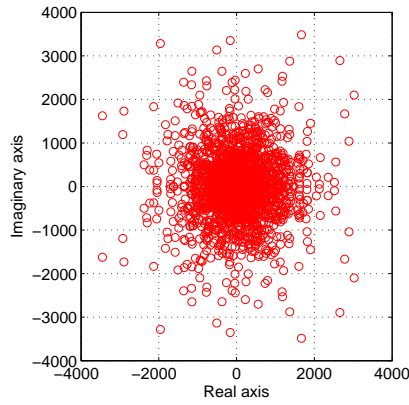


FIG. 8: Distribution of the Fourier coefficients in the complex plane corresponding to the chaotic signal x_1 for $H = 0.2$, $N = 1.5$ and $k = 0.8$.

- [6] A. P. Misra and P. K. Shukla, Phys. Rev. E 79, 056401 (2009).
- [7] F. Haas and P. K. Shukla, Phys. Rev. E 79, 066402 (2009).
- [8] G. Simpson, C. Sulem and P. L. Sulem, Phys. Rev. E 80,

056405 (2009).

- [9] X. Y. Tang and P. K. Shukla, Phys. Scr. 76, 665 (2007).
- [10] M. A. Abdou and E. M. Abulwafa, Z. Naturforsch., A: Phys. Sci. 63a, 646 (2008).
- [11] S. A. El-Wakil and M. A. Abdou, Nonlinear Anal. Theory, Methods Appl. 68, 235 (2008).
- [12] R. P. Sharma, K. Batra and A. D. Verga, Phys. Plasmas 12, 022311 (2005).
- [13] K. Batra, R. P. Sharma and A. D. Verga, J. Plasma Phys. 72, 671 (2006).
- [14] A. Wolf, J. B. Swift, H. L. Swinney, and J. A. Vastano, Physica D 16, 285 (1985).
- [15] For numerical computation of the Lyapunov exponents we have used the guideline program by J. C. Sprott in <http://sprott.physics.wisc.edu/chaos/lespec.htm>.
- [16] A. S. Pikovskii, J. Radiophys. and Quantum Electron. 29, 1438 (1986).
- [17] The MATLAB codes used to compute the amplitude and the phase are as follows:
`h=fft(g); m=abs(h); p=unwrap(angle(h)); % Plot the magnitude and phase.`
`f=(0:length(g)-1)*100/length(h); subplot(2,1,1),`
`plot(f,m); ylabel('Abs. Magnitude'), grid on;`
`subplot(2,1,2), plot(f,p*180/pi); ylabel('Phase [De-`
`grees]'),grid on; xlabel('Frequency [Hertz]');`
- [18] S. Kodba, M. Perc, and M. Marhl, Eur. J. Phys. 26, 205 (2005).